Pergamon

Int. J. Solids Structures Vol. 31, No. 11, pp. 1565–1584, 1994
Elsevier Science Ltd
Printed in Great Britain
0020-7683/94 $7.00 + .00

0020-7683(93)E0029-H

APPLICATION OF TANGENT DERIVATIVE BOUNDARY INTEGRAL EQUATIONS TO THE FORMULATION OF HIGHER ORDER BOUNDARY ELEMENTS

K. H. MUCI-KÜCHLER
Departamento de Ingeniería Mecánica, I.T.E.S.M., Campus Monterrey, 64849 Monterrey, NL, México

and

T. J. RUDOLPHI
Department of Aerospace Engineering and Engineering Mechanics, Iowa State University, Ames, IA 50011-2020, U.S.A.

(*Received* 4 *August* 1992; *in revised form* 18 *November* 1993)

Abstract—Higher order elements with additional degrees of freedom are implemented for three-dimensional elastostatic problems through the coincident collocation of regularized forms of the displacement and the tangent derivative boundary integral equations. The nodal values of the displacements, the tractions and their tangential derivatives with respect to two orthogonal directions are used as the degrees of freedom associated with the functional representation of the boundary variables. Since the surface gradients of the displacements at the collocation points are immediately recovered from the boundary solution, all the stress components are directly obtained at those locations. To demonstrate the accuracy and utility of this approach, a test case is presented in which the results provided by incomplete quartic elements are compared to the ones obtained using the quadratic elements of the "serendipity" family. The methodology presented here is general and can be easily extended to other problems amenable to a boundary integral formulation.

INTRODUCTION

The conventional boundary integral equations are usually obtained from the interior representation for the displacements by letting the source point go to a point on the boundary. If r denotes the distance between the source and the field points and d specifies the number of space dimensions, the stronger singularities contained in the kernels of these equations are $O(r^{1-d})$ in the limit as $r \to 0$ and the Cauchy principal value (CPV) concept can be used to render meaning to the integrals in which they appear. The normal and tangent derivative boundary integral equations arise as limit forms of the gradient of the interior representation for the displacements with respect to the source point coordinates. These equations are termed "hypersingular" since they involve kernels which are $O(r^{-d})$ in the limit as $r \to 0$, but the limits of these representations do exist. The integrals containing such kernels can be interpreted in the sense of the finite part as proposed by Hadamard (1923), since they do not exist in a CPV sense.

The derivative boundary integral equations have been of significant importance in many applications and different alternatives to overcome the difficulties asssociated with their numerical implementation have been summarized by Lutz *et al.* (1991). For the case of open regions, Krishnasamy *et al.* (1990) have shown that the integrals associated with the hypersingular kernels can be computed without relying on a finite part interpretation. Here, before the limit is taken to form a normal derivative (traction) boundary integral equation, the first two terms in a Taylor series expansion of the density function in the hypersingular integrals are subtracted and added back. Then use is made of Stokes' theorem to "convert" these added back terms into regular line integrals and less severely singular integrals on the open surface. For the case of closed domains, Rudolphi (1991) and Liu and Rudolphi (1991) have taken another approach in which certain integral identities

pertaining to the fundamental solution and its derivatives were used instead of Stokes' theorem to reduce the singularity of the added back terms. In both instances, the most strongly singular integral resulting from the added back terms contained a singularity comparable to the weaker kernel of the representation and, by direct association of these terms, the weaker kernel was regularized as well. Although the resulting boundary integrals were analytically regularized, for the case of elasticity they mixed the different boundary variable types making them not well suited for numerical treatment.

However, Rudolphi and Muci-Küchler (1991) have presented completely regularized forms of the derivative equations for two-dimensional elasticity (closed domains) in which only the displacements, the tractions and the tangential derivative of the displacements appeared in the resulting expressions. Here, since only the "tangent part" of the Taylor series expansion was used in the regularization of the hypersingular integrals, the weaker kernels were regularized independently and, in the case of the tangent derivative equations, the integrability theorem was also employed. The final equations contained no singularities and all the integrals could be evaluated using the standard Gaussian quadrature formulae. The same methodology was extended by Muci-Küchler and Rudolphi (1993a) to three-dimensional elasticity where it was necessary to use a form of Stokes' theorem in the derivation of the tangent derivative equations and the resulting expressions contained only weak $O(r^{-1})$ singularities. It should be mentioned that other regularizations of the derivative boundary integral equations, like the one presented by Sladek *et al.* (1993), are also possible.

In elasticity the hypersingular boundary integral equations commonly used are the traction equations. They have been found to be especially useful in problems involving overlapping or crack-like surfaces where the displacement equations are degenerate. In these situations, the displacement and the traction equations play a complementary role since they are collocated at the same spatial locations but on surfaces with opposite normal directions. However, on portions of a boundary with a unique normal direction, it has been shown that the displacement and the traction equations are not independent and, consequently, they cannot be simultaneously collocated at the same boundary points.

Nevertheless, when the point collocation method is used to solve the boundary integral equations, the tangent derivative equations are numerically independent of the displacement and traction equations and thus can be simultaneously collocated with either of them at the same boundary points. Watson (1986) used this idea to construct isoparametric Hermitian cubic boundary elements for plane strain problems. The numerical implementation presented there was cumbersome, since a regularization process was not explicitly employed to obtain a form of the derivative equations in which the singularities of the kernels were removed. For the potential problem and for two-dimensional elasticity Rudolphi (1989) and Muci-Küchler and Rudolphi (1993b) have used regularized forms of the tangent derivative equations to construct higher order elements through the coincident collocation of the conventional and the tangent derivative equations. Here, additional degrees of freedom were incorporated in the approximation of the field variables without inroducing additional collocation points and the tangent derivative equations provided the required extra equations. For the elastostatic case, the nodal values of the displacements, the tractions and their tangential derivatives were used as the degrees of freedom associated with the Hermitian elements. In this fashion, the tangential derivatives of the boundary variables were directly recovered at the collocation points with commensurate accuracy as the primitive variables. Consequently, the tangential strain, and hence the boundary stresses, were determined without employing the derivatives of the interpolation functions.

Krishnasamy *et al.* (1992) have addressed the continuity requirements that should be satisfied in order to use the derivative boundary integral equations. Theoretically, a sufficient condition for the hypersingular integrals to exist is that the density functions must be $C^{1,\alpha}$ (i.e. have Hölder continuous first derivatives) in the neighborhood of the source point. Consequently, with the conventional boundary elements, the completely discontinuous ones have been used in conjunction with the derivative equations since at interior points the functional representation is C^{∞}. Also, several types of C^{1} continuous boundary elements have been employed to allow the collocation of the derivative equations at element interfaces. In particular, for three-dimensional problems, Liu and Rizzo (1991) have successfully

used Overhauser C^1 continuous boundary elements for the solution of acoustic wave problems.

In this paper, higher order elements with additional degrees of freedom for three-dimensional elasticity are implemented through the coincident collocation of the conventional and the tangent derivative boundary integral equations. These elements include nodal values of the tangential derivatives of the displacements and the tractions in two orthogonal directions as part of the interpolation of the boundary variables and they only provide C^1 continuity at the collocation points when they are located at element interfaces. As in the two-dimensional case, at the locations where the tangent derivative equations are collocated, the boundary stresses are immediately recovered from the boundary solution.

THE CONVENTIONAL AND TANGENT DERIVATIVE BOUNDARY INTEGRAL EQUATIONS

For a closed domain bounded by a surface S, the representation integral for the displacements in three-dimensional elasticity can be written in the following form (Liu and Rudolphi, 1991)

$$\int_S T_{ij}(\mathbf{x}, \boldsymbol{\xi})\{u_j(\mathbf{x}) - u_j(\boldsymbol{\xi})\}\, \mathrm{d}S(\mathbf{x}) = \int_S U_{ij}(\mathbf{x}, \boldsymbol{\xi}) t_j(\mathbf{x})\, \mathrm{d}S(\mathbf{x}), \tag{1}$$

where $\mathbf{x} = (x_1, x_2, x_3)$ and $\boldsymbol{\xi} = (\xi_1, \xi_2, \xi_3)$ denote the field and source point coordinates, u_i and t_i are the displacement and traction components, and the kernels U_{ij} and T_{ij} correspond to the fundamental solution displacement and traction tensors. For isotropy, the fundamental tensors are given by

$$U_{ij}(\mathbf{x}, \boldsymbol{\xi}) = \frac{1}{16\pi\mu(1-\nu)}\left(\frac{1}{r}\right)[(3-4\nu)\delta_{ij} + r_{,i}r_{,j}] \tag{2}$$

$$T_{ij}(\mathbf{x}, \boldsymbol{\xi}) = \frac{-1}{8\pi(1-\nu)}\left(\frac{1}{r^2}\right)\left\{\frac{\partial r}{\partial n}[(1-2\nu)\delta_{ij} + 3r_{,i}r_{,j}] + (1-2\nu)(r_{,j}n_i - r_{,i}n_j)\right\}, \tag{3}$$

where $T_{ij} = E_{jklm}n_k U_{il,m}$ and $E_{ijkl} = \lambda\delta_{ij}\delta_{kl} + \mu(\delta_{ik}\delta_{jl} + \delta_{il}\delta_{jk})$ is the fourth-order material property tensor describing the elastic medium. Lamé's constants are denoted by λ and μ, ν is Poisson's ratio, n_i are the components of the unit outward normal to the boundary S at the field point $\mathbf{x}$, $r = |\mathbf{x} - \boldsymbol{\xi}|$ is the distance between the source and the field point and $r_{,i} = (x_i - \xi_i)/r$. Here, the comma notation has been used to indicate differentiation with respect to the coordinates at $\mathbf{x}$. This convention will be followed in the sequel while differentiation with respect to the coordinates at $\boldsymbol{\xi}$, wherever it occurs, will be always explicitly written out.

If the displacement components are continuous in the vicinity of the source point $\boldsymbol{\xi}$, the difference $u_i(\mathbf{x}) - u_i(\boldsymbol{\xi})$ is $O(r)$ in the limit as $r \to 0$ and the integrands in eqn (1) contain only weak $O(1/r)$ singularities. Consequently, one can let the interior point $\boldsymbol{\xi}$ go to a point $\mathbf{z}$ on the boundary to obtain the following regularized form of the conventional boundary integral equation

$$\int_S T_{ij}(\mathbf{x}, \mathbf{z})\{u_j(\mathbf{x}) - u_j(\mathbf{z})\}\, \mathrm{d}S(\mathbf{x}) = \int_S U_{ij}(\mathbf{x}, \mathbf{z}) t_j(\mathbf{x})\, \mathrm{d}S(\mathbf{x}). \tag{4}$$

To determine the tangent derivative boundary integral equations some geometry related quantities need to be defined. Let $\boldsymbol{\nu}$ denote the unit outward normal to the boundary S at the limit point $\mathbf{z}$ and let $(\boldsymbol{\zeta}_1, \boldsymbol{\zeta}_2, \boldsymbol{\zeta}_3 = \boldsymbol{\nu})$ be a proper orthonormal basis as shown in Fig.

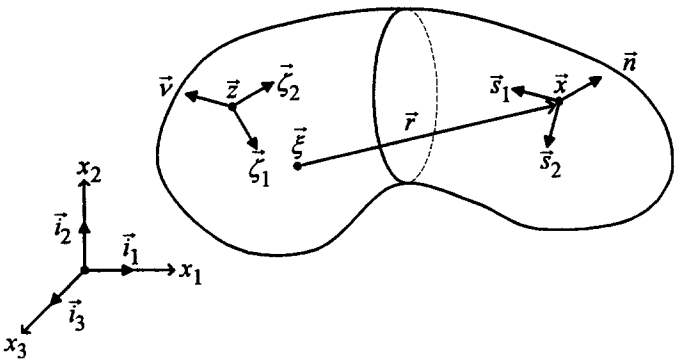

Fig. 1. Three-dimensional domain and coordinate systems.

1. Here, the two unit tangent vectors ζ_1 and ζ_2 can be arbitrarily chosen as long as they satisfy the condition $\zeta_1 \times \zeta_2 = \nu$. The direction cosines of the basis vectors ζ_1, ζ_2, and ζ_3 with respect to the underlying rectangular coordinate system x_1, x_2, x_3 will be determined and denoted by $l_{ij} = \zeta_i \cdot \mathbf{i}_j$.

Also, in the sequel, ε_{ijk} will be the three-dimensional unit pseudotensor, $\varepsilon_{\alpha\beta}$ will denote the two-dimensional unit pseudotensor ($\varepsilon_{11} = \varepsilon_{22} = 0, \varepsilon_{12} = -\varepsilon_{21} = 1$) and it is understood that the range of the Greek indices is only from 1 to 2 and that the summation convention is in force.

To obtain the form of the interior representation of the displacement gradients that leads to the tangent derivative boundary integral equations, the operation

$$(\zeta_\beta \times \nu) \cdot \nabla_\xi = \varepsilon_{pqk} \nu_q l_{\beta p} \frac{\partial}{\partial \xi_k}, \quad \beta = 1, 2 \tag{5}$$

is applied to the representation integral for the displacements and use is made of certain identities pertaining to the fundamental tensors and their derivatives to regularize the resulting expression. A detailed derivation was given by Muci-Küchler and Rudolphi (1993a) and the final equation can be written as

$$\int_S V_{\beta ij}(\mathbf{x}, \xi)\left[u_j(\mathbf{x}) - u_j(\xi) - \frac{\partial u_j}{\partial \zeta_\alpha}(\xi) l_{\alpha l} r_l\right] \mathrm{d}S(\mathbf{x}) + \int_S Y_{\beta ij\alpha}(\mathbf{x}, \xi)\, \mathrm{d}S(\mathbf{x}) \frac{\partial u_j}{\partial \zeta_\alpha}(\xi)$$

$$= \int_S [W^0_{\beta ij}(\mathbf{x}, \xi) t_j(\mathbf{x}) - W_{\beta ij}(\mathbf{x}, \xi) t_j(\xi)]\, \mathrm{d}S(\mathbf{x}), \quad \beta = 1, 2, \tag{6}$$

where

$$V_{\beta ij}(\mathbf{x}, \xi) = -\varepsilon_{\beta\gamma} l_{\gamma k} \frac{\partial T_{ij}}{\partial \xi_k}(\mathbf{x}, \xi) \tag{7}$$

$$W^0_{\beta ij}(\mathbf{x}, \xi) = l_{\beta p} \varepsilon_{pqk} \nu_q \frac{\partial U_{ij}}{\partial \xi_k}(\mathbf{x}, \xi) \tag{8}$$

$$W_{\beta ij}(\mathbf{x}, \xi) = l_{\beta p} \varepsilon_{pqk} n_q(\mathbf{x}) \frac{\partial U_{ij}}{\partial \xi_k}(\mathbf{x}, \xi) \tag{9}$$

$$Y_{\beta ij\alpha}(\mathbf{x}, \xi) = \lambda l_{\alpha j}[n_m(\mathbf{x}) W^0_{\beta im}(\mathbf{x}, \xi) - \nu_m W_{\beta im}(\mathbf{x}, \xi)] + \mu l_{\alpha m} n_m(\mathbf{x}) W^0_{\beta ij}(\mathbf{x}, \xi)$$
$$+ \mu l_{\alpha m}[n_j(\mathbf{x}) W^0_{\beta im}(\mathbf{x}, \xi) - \nu_j W_{\beta im}(\mathbf{x}, \xi)]. \tag{10}$$

From eqns (7)–(10) it is seen that the kernel $V_{\beta ij}$ is $O(1/r^3)$ or hypersingular in the limit as $r \to 0$ while $W_{\beta ij}$ and $W^0_{\beta ij}$ are both strongly singular or $O(1/r^2)$ and $Y_{\beta ij\alpha}$ is $O(1/r)$

provided that the boundary S has a continuous unit outward normal at the limit point $\mathbf{z}$. However, if at the source point $\boldsymbol{\xi}$ the displacements have Hölder continuous first derivatives and the tractions are continuous, and if the geometry is smooth at the point $\mathbf{z}$, all the terms in eqn (6) will contain at most weak $O(1/r)$ singularities. Thus, one can let $\boldsymbol{\xi} \to \mathbf{z} \in S$ to obtain the following tangent derivative boundary integral equations

$$\int_S V_{\beta ij}\left[u_j - u_j(\mathbf{z}) - \frac{\partial u_j}{\partial \zeta_\alpha}(\mathbf{z}) l_{al} r_l\right] \mathrm{d}S + \int_S Y_{\beta ij\alpha}\,\mathrm{d}S \frac{\partial u_j}{\partial \zeta_\alpha}(\mathbf{z}) = \int_S [W^0_{\beta ij} t_j - W_{\beta ij} t_j(\mathbf{z})]\,\mathrm{d}S, \quad \beta = 1,2. \tag{11}$$

In the sequel, the spatial arguments of the functions will not be explicit with the understanding that the arguments of the two point functions are always $(\mathbf{x}, \mathbf{z})$ and the argument of the other functions is $(\mathbf{x})$ unless explicitly noted otherwise.

NUMERICAL IMPLEMENTATION

The method of point collocation is used to solve the conventional and the tangent derivative boundary integral equations presented in the previous section. The surface point $\mathbf{z}$ becomes the collocation point and it is convenient to rearrange eqns (4) and (11) in the following fashion

$$\int_{S'} T_{ij} u_j \,\mathrm{d}S + \int_{S_0} T_{ij}[u_j - u_j(\mathbf{z})]\,\mathrm{d}S - \int_{S'} T_{ij}\,\mathrm{d}S\, u_j(\mathbf{z}) = \int_{S'} U_{ij} t_j \,\mathrm{d}S + \int_{S_0} U_{ij} t_j \,\mathrm{d}S \tag{12}$$

$$\int_{S'} V_{\beta ij} u_j \,\mathrm{d}S + \int_{S_0} V_{\beta ij}\left[u_j - u_j(\mathbf{z}) - \frac{\partial u_j}{\partial \zeta_\alpha}(\mathbf{z}) l_{al} r_l\right] \mathrm{d}S - \int_{S'} V_{\beta ij}\,\mathrm{d}S\, u_j(\mathbf{z}) + \left\{\int_{S'} Y_{\beta ij\alpha}\,\mathrm{d}S + \int_{S_0} Y_{\beta ij\alpha}\,\mathrm{d}S - \int_{S'} V_{\beta ij} l_{\alpha l} r_l \,\mathrm{d}S\right\} \frac{\partial u_j}{\partial \zeta_\alpha}(\mathbf{z})$$
$$= \int_{S'} W^0_{\beta ij} t_j \,\mathrm{d}S + \int_{S_0} [W^0_{\beta ij} t_j - W_{\beta ij} t_j(\mathbf{z})]\,\mathrm{d}S - \int_{S'} W_{\beta ij}\,\mathrm{d}S\, t_j(\mathbf{z}), \quad \beta = 1,2, \tag{13}$$

where we have separated the total boundary S into two parts: one denoted by S_0 which contains the collocation point $\mathbf{z}$ and the remainder denoted by S'.

In eqns (12) and (13) the integrals along S' are integrable in the ordinary sense since their integrands contain no singularities. However, the terms in the integrals along S_0 contain at most $O(1/r)$ singularities, but they are easily removed using polar coordinates after mapping the actual surface into a two-dimensional space.

Then by the boundary element method, the surface of the domains is discretized or divided into elements and the two different types of approximations of this process are carefully delineated. First, the actual geometry associated with each element is represented using a set of predefined shape or interpolation functions and a set of known geometric parameters. Second, on a given element, the behavior of the field variables is approximated through the use of shape functions and "generalized coordinates" or "nodal degrees of freedom". Thus, in a general sense, the geometric and the functional representations associated with a given element are independent approximations. Although it is common practice to use isoparametric elements in which the geometry and the field variables are interpolated by the same set of shape functions, this approach is not convenient for elements with a discontinuous or partially discontinuous functional representation or when the field variables are interpolated using polynomials of high order.

In the present implementation, the geometry and the field variables are approximated on the elements using completely different sets of shape functions. The coordinates on an element are determined by

$$x_i = \sum_{J=1}^{n} N_J(\eta_1, \eta_2)[x_i]^J, \quad i = 1, 2, 3, \tag{14}$$

where η_1 and η_2 are intrinsic coordinates, n is the number of geometric nodes on the element, $N_J(\eta_1, \eta_2)$ are shape functions, and $[x_i]^J$ denotes the ith coordinate of the Jth geometric node. The particular choice of the shape functions depends only on the surface to be approximated.

The type of interpolation functions for the approximation of the field variables on a given element depends on the number of independent equations available at each collocation point or functional node. In the usual boundary element method only the conventional boundary integral equations (12) are collocated at each functional node and the displacements u_i (and similarly the tractions t_i) are approximated by

$$u_i = \sum_{J=1}^{m} M_J(\eta_1, \eta_2)[u_i]^J, \quad i = 1, 2, 3, \tag{15}$$

where m is the number of functional nodes on the element, $M_J(\eta_1, \eta_2)$ are the conventional shape functions and $[u_i]^J$ is the ith displacement at the Jth functional node. By eqn (15) there are three degrees of freedom associated with each functional node and eqns (12) are the requisite equations to determine three unknowns at each node by collocation. However, since the six tangent derivative boundary integral equations (13) are numerically independent of the three displacement equations (12), it is possible to simultaneously collocate all nine equations at the same spatial locations in order to formulate higher order elements.

By this approach, the stronger continuity requirements of the derivative equations take precedence over the ones imposed by the displacement equations and, consequently, proper element and collocation point selection must be observed. The shape functions used to interpolate the field variables should provide first derivative continuity of the displacements u_i and zeroth derivative continuity of the tractions t_i at the collocation points. Also, the approximation of the geometry at those locations should be sufficiently smooth so as to guarantee continuity of the tangent vectors.

With nine equations collocated at each one of the functional nodes of an element, it is possible to incorporate the nodal values of the surface gradients of the displacements and the tractions into the interpolation of the field variables. For that purpose, orthonormal basis $(\mathbf{s}_1, \mathbf{s}_2, \mathbf{n})$ are introduced at each of the functional nodes of the element. Since the two unit tangent vectors $\mathbf{s}_1$ and $\mathbf{s}_2$ can be arbitrary provided that $\mathbf{s}_1 \times \mathbf{s}_2 = \mathbf{n}$, $\mathbf{s}_1^J$ and $\mathbf{s}_2^J$ are identified as the two particular directions associated with the Jth functional node and $\zeta_1 = \mathbf{s}_1^J$ and $\zeta_2 = \mathbf{s}_2^J$ are used to denote tangent directions when the tangent derivative equations (13) are collocated there. Furthermore, if several neighboring elements share the same functional node, then all will use the same unit vectors $\mathbf{s}_1$ and $\mathbf{s}_2$ at that particular location. With these considerations in mind, the functional representation of the displacements and the tractions over an element are written as

$$u_i = \sum_{J=1}^{m} \left\{ H_0^J(\eta_1, \eta_2)[u_i]^J + H_1^J(\eta_1, \eta_2)\left[\frac{\partial u_i}{\partial s_1^J}\right]^J + H_2^J(\eta_1, \eta_2)\left[\frac{\partial u_i}{\partial s_2^J}\right]^J \right\} \tag{16}$$

$$t_i = \sum_{J=1}^{m} \left\{ H_0^J(\eta_1, \eta_2)[t_i]^J + H_1^J(\eta_1, \eta_2)\left[\frac{\partial t_i}{\partial s_1^J}\right]^J + H_2^J(\eta_1, \eta_2)\left[\frac{\partial t_i}{\partial s_2^J}\right]^J \right\}. \tag{17}$$

In these expressions the three shape functions H_0^J, H_1^J, and H_2^J associated with the Jth functional node are such that

$$H_0^J(\eta_1^K, \eta_2^K) = \begin{cases} 1, & \text{for } K = J \\ 0, & \text{for } K \neq J \end{cases}$$

$$\frac{\partial H_0^J}{\partial s_1^K}(\eta_1^K, \eta_2^K) = \frac{\partial H_0^J}{\partial s_2^K}(\eta_1^K, \eta_2^K) = 0, \quad \text{for all } K \tag{18}$$

$$\frac{\partial H_1^J}{\partial s_1^K}(\eta_1^K, \eta_2^K) = \begin{cases} 1, & \text{for } K = J \\ 0, & \text{for } K \neq J \end{cases}$$

$$H_1^J(\eta_1^K, \eta_2^K) = \frac{\partial H_1^J}{\partial s_2^K}(\eta_1^K, \eta_2^K) = 0, \quad \text{for all } K \tag{19}$$

$$\frac{\partial H_2^J}{\partial s_2^K}(\eta_1^K, \eta_2^K) = \begin{cases} 1, & \text{for } K = J \\ 0, & \text{for } K \neq J \end{cases}$$

$$H_2^J(\eta_1^K, \eta_2^K) = \frac{\partial H_2^J}{\partial s_1^K}(\eta_1^K, \eta_2^K) = 0, \quad \text{for all } K \tag{20}$$

where $K = 1, 2, \ldots, m$ and η_1^K and η_2^K represent the local coordinates of the Kth functional node.

From eqns (18)–(20) it can be seen that the shape functions H_0^J, H_1^J, and H_2^J ($J = 1, 2, \ldots, m$) must be related to geometric parameters associated with an element. Consequently, the complete set of shape functions should be established individually for each element in the discretization of the domain. However, the process of finding these interpolation functions is relatively easy since they can be computed numerically through the use of the "geometry independent" shape functions $\hat{H}_0^J$, $\hat{H}_1^J$, and $\hat{H}_2^J$ ($J = 1, 2, \ldots, m$) that satisfy the following conditions

$$\hat{H}_0^J(\eta_1^K, \eta_2^K) = \begin{cases} 1, & \text{for } K = J \\ 0, & \text{for } K \neq J \end{cases}$$

$$\frac{\partial \hat{H}_0^J}{\partial \eta_1}(\eta_1^K, \eta_2^K) = \frac{\partial \hat{H}_0^J}{\partial \eta_2}(\eta_1^K, \eta_2^K) = 0, \quad \text{for all } K \tag{21}$$

$$\frac{\partial \hat{H}_1^J}{\partial \eta_1}(\eta_1^K, \eta_2^K) = \begin{cases} 1, & \text{for } K = J \\ 0, & \text{for } K \neq J \end{cases}$$

$$\hat{H}_1^J(\eta_1^K, \eta_2^K) = \frac{\partial \hat{H}_1^J}{\partial \eta_2}(\eta_1^K, \eta_2^K) = 0, \quad \text{for all } K \tag{22}$$

$$\frac{\partial \hat{H}_2^J}{\partial \eta_2}(\eta_1^K, \eta_2^K) = \begin{cases} 1, & \text{for } K = J \\ 0, & \text{for } K \neq J \end{cases}$$

$$\hat{H}_2^J(\eta_1^K, \eta_2^K) = \frac{\partial \hat{H}_2^J}{\partial \eta_1}(\eta_1^K, \eta_2^K) = 0, \quad \text{for all } K. \tag{23}$$

The relationship between the two sets of shape functions mentioned above can be established through the expression that relates the derivatives of H_0^J, H_1^J, and H_2^J with respect to the local coodinates η_1 and η_2 to the derivatives of the shape functions in the directions given by $\mathbf{s}_1$ and $\mathbf{s}_2$. Using the results of Appendix A one can write

$$\begin{Bmatrix} \dfrac{\partial H_L^J}{\partial s_1} \\ \dfrac{\partial H_L^J}{\partial s_2} \end{Bmatrix} = \frac{1}{G}\begin{bmatrix} (g_{22}\mathbf{e}_1 - g_{12}\mathbf{e}_2)\cdot\mathbf{s}_1 & (g_{11}\mathbf{e}_2 - g_{21}\mathbf{e}_1)\cdot\mathbf{s}_1 \\ (g_{22}\mathbf{e}_1 - g_{12}\mathbf{e}_2)\cdot\mathbf{s}_2 & (g_{11}\mathbf{e}_2 - g_{21}\mathbf{e}_1)\cdot\mathbf{s}_2 \end{bmatrix}\begin{Bmatrix} \dfrac{\partial H_L^J}{\partial \eta_1} \\ \dfrac{\partial H_L^J}{\partial n_2} \end{Bmatrix} \tag{24}$$

$$\begin{Bmatrix} \dfrac{\partial H_L^J}{\partial s_1} \\ \dfrac{\partial H_L^J}{\partial s_2} \end{Bmatrix} = \begin{bmatrix} A_{11} & A_{12} \\ A_{21} & A_{22} \end{bmatrix}\begin{Bmatrix} \dfrac{\partial H_L^J}{\partial \eta_1} \\ \dfrac{\partial H_L^J}{\partial \eta_2} \end{Bmatrix}, \tag{25}$$

where $\mathbf{e}_\alpha = (\partial x_k/\partial n_\alpha)\mathbf{i}_k$ are basis vectors related to the local coordinates, $g_{\alpha\beta} = \mathbf{e}_\alpha \cdot \mathbf{e}_\beta$ denote "surface components" of the metric tensor, $G = \det(g_{\alpha\beta})$ and $L = 0, 1, 2$.

From eqns (21)–(23), together with eqn (25), it is seen that eqns (18)–(20) are satisfied by the choices of

$$H_0^J(\eta_1, \eta_2) = \hat{H}_0^J(\eta_1, \eta_2) \tag{26}$$

$$H_1^J(\eta_1, \eta_2) = \frac{1}{[A]^J}\{[A_{22}]^J \hat{H}_1^J(\eta_1, \eta_2) - [A_{21}]^J \hat{H}_2^J(\eta_1, \eta_2)\} \tag{27}$$

$$H_2^J(\eta_1, \eta_2) = \frac{1}{[A]^J}\{[A_{11}]^J \hat{H}_2^J(\eta_1, \eta_2) - [A_{12}]^J \hat{H}_1^J(\eta_1, \eta_2)\}, \tag{28}$$

where $A = A_{11}A_{22} - A_{12}A_{21}$ and the notation $[\cdot]^J$ is used to specify quantities evaluated at the Jth functional node.

The four terms $A_{\alpha\beta}$ can be computed at each one of the functional nodes of an element if the components $\partial x_i/\partial \eta_\alpha$ of the basis vectors $\mathbf{e}_\alpha$ can be determined at those locations. This task poses no difficulty since it can be accomplished using the geometric representations of the element. From eqn (14) it is immediate that

$$\frac{\partial x_i}{\partial \eta_\alpha} = \sum_{J=1}^{n} \frac{\partial N_J}{\partial \eta_\alpha}(\eta_1, \eta_2)[x_i]^J, \quad i = 1, 2, 3. \tag{29}$$

Alternately, since the shape functions $\hat{H}_0^J$, $\hat{H}_1^J$, and $\hat{H}_2^J$ are related only to the parametric coordinates η_1 and η_2, they can be established on the intrinsic element in the customary fashion. For completeness, the interpolation functions for several higher order elements are presented in Appendix B.

The methodology presented here is general and can be used to implement higher order elements of different shapes and with any number of nodes. Also, no inversion is necessary in order to obtain the shape functions H_0^J, H_1^J, H_2^J associated with a specific element in the discretization of the domain. These shape functions exist as long as the geometric description of the element is such that the transformation from the global space to the intrinsic element coordinates is well defined (the determinant of $g_{\alpha\beta}$ is neither zero nor infinity).

If the conventional boundary integral equations (12) are collocated at every functional node in the domain, the tangent derivative equations (13) can be simultaneously collocated with them only at those locations where the higher order elements are used. Thus, it is possible to mix different functional element types in a given mesh so that the higher order elements are only used in the areas where the field variables exhibit rapid changes or where the tangential displacement or traction gradients are desired.

COMPUTATION OF THE STRESSES ON THE SURFACE

Once the boundary element solution has been obtained, it is possible to find the stress and the strain tensors at any location on the boundary S through the functional representation on the elements. The details on how these quantities are determined can be found in Sladek and Sladek (1986) and also in Aliabadi and Rooke (1991). For the case of the functional nodes of an element, a system of rectangular coordinates x'_1, x'_2, x'_3 is introduced at the particular node under consideration, the orthonormal basis $(\mathbf{s}_1, \mathbf{s}_2, \mathbf{n})$ is identified with the basis $(\mathbf{i}'_1, \mathbf{i}'_2, \mathbf{i}'_3)$ of the primed system and the coefficients of the transformation (from the unprimed basis to the primed one) are defined as $Q_{k'm} = \mathbf{i}'_k \cdot \mathbf{i}_m$.

After the boundary solution for a given model, the displacement and the traction vectors $\mathbf{u} = u_k \mathbf{i}_k$ and $\mathbf{t} = t_k \mathbf{i}_k$ are known at each of the functional nodes of both the conventional and the higher order elements. Consequently, the stress components on the plane whose unit outward normal is $\mathbf{n}$ are directly given by

$$\sigma'_{3k} = Q_{k'm} t_m. \tag{30}$$

Also, the strain components ε'_{11}, ε'_{22}, and $\varepsilon'_{12} = \varepsilon'_{21}$ can be found through the expression

$$\varepsilon'_{\alpha\beta} = \frac{1}{2}\left[Q_{\alpha' m} \frac{\partial u_m}{\partial x'_\beta} + Q_{\beta' m} \frac{\partial u_m}{\partial x'_\alpha} \right] = \frac{1}{2}\left[(\mathbf{s}_\alpha \cdot \mathbf{i}_m) \frac{\partial u_m}{\partial s_\beta} + (\mathbf{s}_\beta \cdot \mathbf{i}_m) \frac{\partial u_m}{\partial s_\alpha} \right] \tag{31}$$

if the values of the tangential derivatives $\partial u_m / \partial s_1$ and $\partial u_m / \partial s_2$ of the displacement components in the unprimed system can be determined at the functional node. From eqn (16) one can see that for the elements described by eqns (16) and (17) the nodal values of the tangential derivatives are a part of the approximation for the displacements and, consequently, they are immediately recovered from the boundary solution. However, for the conventional elements, these quantities must be established through the nodal values of the displacements and the derivatives of the shape functions M_J with respect to the parametric coordinates η_1 and η_2.

Using the results presented in Appendix A we have

$$\frac{\partial u_i}{\partial s_\alpha} = \frac{1}{G}\left[(g_{22}\mathbf{e}_1 - g_{12}\mathbf{e}_2) \frac{\partial u_i}{\partial \eta_1} + (g_{11}\mathbf{e}_2 - g_{21}\mathbf{e}_1) \frac{\partial u_i}{\partial \eta_2} \right] \cdot \mathbf{s}_\alpha, \tag{32}$$

where the values of $\partial u_i / \partial \eta_1$ and $\partial u_i / \partial \eta_2$ can be determined from eqn (15) as

$$\frac{\partial u_i}{\partial \eta_\alpha} = \sum_{J=1}^{m} \frac{\partial M_J}{\partial \eta_\alpha}(\eta_1, \eta_2)[u_i]^J. \tag{33}$$

Finally, the remaining unknown stresses and strains in the primed system can be obtained using Hooke's law, and their counterparts in the unprimed system are readily determined through the transformation law for second-order tensors.

The procedure used here to compute the stress and strain states at the functional nodes of the higher order elements exhibits a major difference relative to that employed for the conventional elements. In the case of the higher order elements, the tangential gradients are incorporated as part of the formulation of the problem and are directly obtained as part of the boundary solution. However, for the conventional elements, these quantities must be established through the derivatives of the functional representation for the displacement components. Of course, the accuracy that can be expected from the two approaches will be different.

In the previous section it was shown that the shape functions H_0^J, H_1^J, and H_2^J associated with the higher order elements are established on an element by element basis using the geometry independent shape functions $\hat{H}_0^J$, $\hat{H}_1^J$, and $\hat{H}_2^J$ together with some geometric parameters related to the specific element under consideration. This may seem to add a

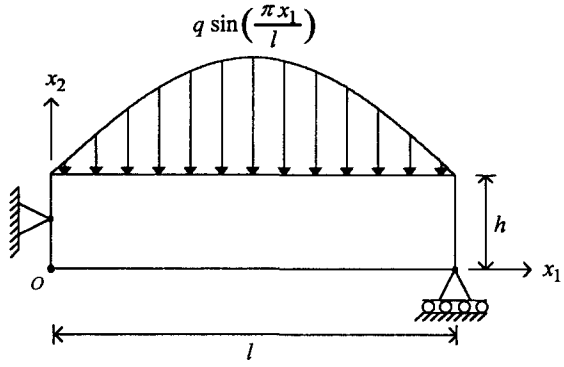

Fig. 2. Simply supported beam subject to a sinusoidal load.

"computational cost" to the higher order elements that is not present for the conventional ones. However, this is not true if the desired output from the boundary element code must include the values of the stresses or the strains at the functional nodes. Comparing eqns (27) and (28) with eqn (32) one can see that for both element types it is necessary to determine $\mathbf{e}_\alpha$, $g_{\alpha\beta}$, and G at each functional node. The only difference is that for the higher order elements this is done during the generation of the system of equations whereas for the conventional elements this is performed as a post-processing task.

The computation of the stress and the strain tensors at surface points that are not functional nodes follows the same procedure for both element types. Here the traction components t_m used in eqn (30) and the displacement gradients $\partial u_m/\partial s_1$ and $\partial u_m/\partial s_2$ needed in eqn (31) must be obtained, respectively, from the functional representation for the traction and the displacement components. Consequently, in this case, the difference in accuracy will be related to the use of a "p" boundary element method instead of an "h" one.

NUMERICAL RESULTS

To demonstrate that the formulation proposed in this paper is computationally stable and to illustrate the accuracy of the higher order elements, the test problem of a simply supported beam subject to a continuously distributed sinusoidal load at its top surface is employed. Figure 2 shows the cross-section of the beam in the x_1x_2 plane and its loading. The length, height, and thickness of the beam are denoted by l, h, and t, respectively. With further boundary conditions applied to the beam such that a state of plane strain prevails inside the elastic medium, an analytical solution for the problem can be found as in Little (1973). Under these circumstances, the only nonzero displacement components are

$$u_1 = a\cos wx_1\{[bw^2x_2-2c(1-\nu)]\cosh wx_2+w[b(1-2\nu)-cx_2]\sinh wx_2\}+d \quad (34)$$

$$u_2 = a\sin wx_1\{-w[2b(1-\nu)+cx_2]\cosh wx_2+[c(1-2\nu)+bw^2x_2]\sinh wx_2\}, \quad (35)$$

where the four constants a, b, c, and d are given by the following expressions

$$a = \frac{2q(1+\nu)}{Ew^2(\cosh 2wh-1-2w^2h^2)} \quad (36)$$

$$b = wh\cosh wh+\sinh wh \quad (37)$$

$$c = w^2h\sinh wh \quad (38)$$

$$d = \frac{a}{2}w(\sinh wh-wh)\left(wh\cosh\frac{wh}{2}-(2-4\nu)\sinh\frac{wh}{2}\right). \quad (39)$$

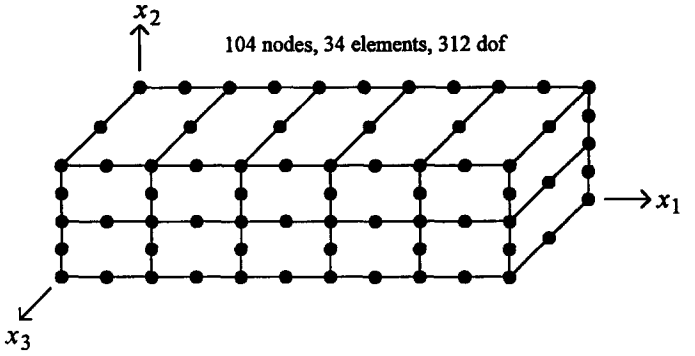

Fig. 3. Mesh for the quadratic "serendipity" elements.

In the above equations, q denotes the magnitude of the sinusoidal load, E is Young's modulus, v is Poisson's ratio, and $w = \pi/l$.

To compare the performance of the higher order elements with the conventional ones, the two models shown in Figs 3 and 4 were used. Note that the geometric nodes of the elements have been omitted and only the functional nodes are displayed. The dimensions of the beam are $l = 10$ and $t = h = 5$ and the material properties are taken as $v = 0.3$ and $E = 200$. The first model consists of 34 elements with 104 functional nodes and 312 degrees of freedom. Here, the shape functions of the continuous quadratic element of the "serendipity" family are used for the functional representation of the field variables whereas the shape functions of the continuous linear element of the "serendipity" family are employed for the approximation of the geometry. For the second model, the mesh consists of 10 elements with 32 functional nodes and 288 degrees of freedom. In this case, the shape functions of the discontinuous and partially discontinuous incomplete quartic elements given in Appendix B are used for the functional representation. Also, as in the first model, the geometry of the elements is approximated using the shape functions of the continuous linear element of the "serendipity" family.

The differences between the two models are evident. Although both meshes have approximately the same number of degrees of freedom, the second with higher order elements has 69% less functional nodes and 71% less elements than the first with conventional elements. On the other hand, from Fig. 4 one can see that none of the functional nodes is located at the edges or corners of the beam, which avoids the problem of a non-unique normal.

In the calculations, the magnitude of the sinusoidal load was chosen as $q = 1$ and the values from the analytical solution were used as boundary conditions for both models. The faces of the beam at $x_3 = 0$ and $x_3 = t$ are subject to the conditions $t_1 = 0$, $t_2 = 0$, and $u_3 = 0$ and the surface at $x_2 = 0$ is traction free. Also at $x_2 = h$, the tractions are specified as $t_1 = 0$, $t_2 = -q \sin wx_1$, and $t_3 = 0$. For the face of the beam at $x_1 = 0$, u_1 is specified

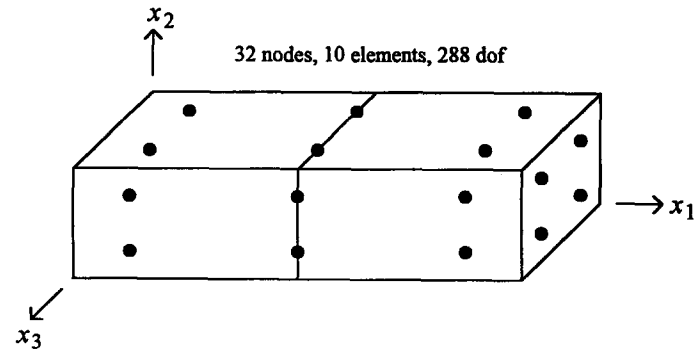

Fig. 4. Mesh for the incomplete quartic elements.

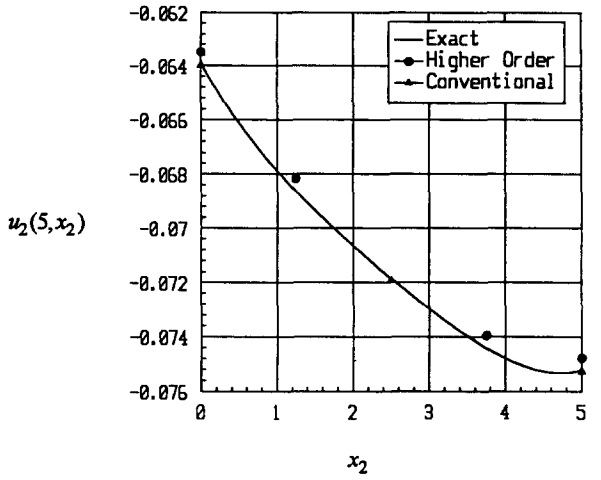

Fig. 5. Vertical displacement on the front face of the beam at $x_1 = 5$.

according to eqn (34) and the remaining conditions are given as $u_2 = 0$ and $t_3 = 0$. Finally, for the surface at $x_1 = l$, the conditions $t_1 = 0$, $u_2 = 0$, and $t_3 = 0$ are prescribed. It should also be mentioned that, whereas for the conventional elements it is only necessary to specify either a displacement or a traction component at every functional node in the domain, for the higher order elements one must also provide the nodal values of the tangential derivatives of the prescribed field variables.

After the primary solution, the values provided by each model are compared to the analytical solution. For the beam example here, all the results are independent of x_3 since the boundary conditions maintain a state of plane strain through the beam. Furthermore, although the values provided by both models are close to the exact solution, some differences in performance between the two element types can be detected.

Results for the vertical displacement u_2 on the front face of the beam at $x_1 = 5$ are shown in Fig. 5. For the higher order elements, the values shown at $x_2 = 0$ and $x_2 = 5$ correspond to nodes located on the bottom and top surfaces of the model. In this case it is seen that the conventional elements provided more accurate values for the displacement component than the higher order elements.

Figure 6 shows a comparison for the traction component t_2 on the right face of the beam. Here the results provided by the conventional elements show some deviation with respect to the analytical ones. However, the values provided by the higher order elements fall almost on the analytical curve.

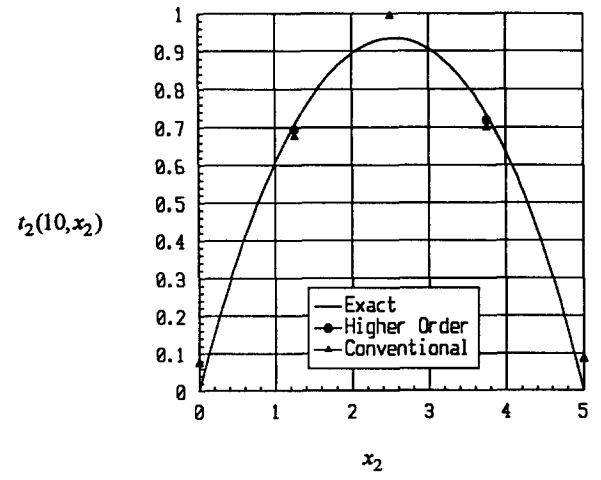

Fig. 6. Vertical traction on the right face of the beam.

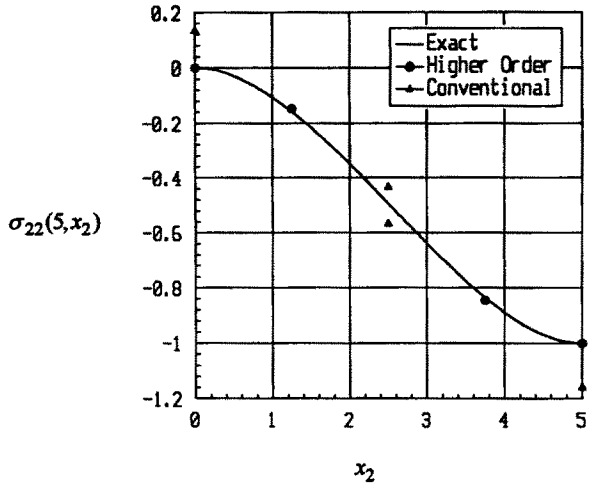

Fig. 7. Normal stress σ_{22} on the front face of the beam at $x_1 = 5$.

For the stress component σ_{22}, the results on the front face of the beam at $x_1 = 5$ and $x_2 = 1.25$ are shown in Figs 7 and 8, respectively. In Fig. 7, the values for the higher order elements shown at $x_2 = 0$ and $x_2 = 5$ correspond to nodes located on the bottom and top surfaces of the model. Also, in Fig. 8, the values for the higher order elements shown at $x_1 = 0$ and $x_1 = 10$ correspond to nodes located on the left and right faces of the beam. For both cases it is seen that the values corresponding to the higher order elements are closer to the analytical solution than the ones for the conventional elements. In addition, these figures show that for the conventional elements the values of σ_{22} are discontinuous across element interfaces.

Figure 9 presents the values for the strain component ε_{22} on the front face of the beam at $x_2 = 3.75$ and Fig. 10 shows a plot for ε_{22} on the top face of the beam. In the case of Fig. 9, the values for the higher order elements at $x_1 = 0$ and $x_1 = 10$ were taken from nodes on the left and right faces of the beam. In both instances the values provided by the higher order elements are in good agreement with the exact solution. However, in Fig. 9 it is seen that the results for the conventional elements deviate significantly from the analytical solution. Also, Fig. 10 reveals that in certain cases the quadratic elements have difficulties to follow concavity of the theoretical curve.

Finally, Fig. 11 shows a comparison for the displacement gradient $\partial u_1/\partial u_2$ on the right face of the beam. Here the data points for the higher order elements fall very close to the

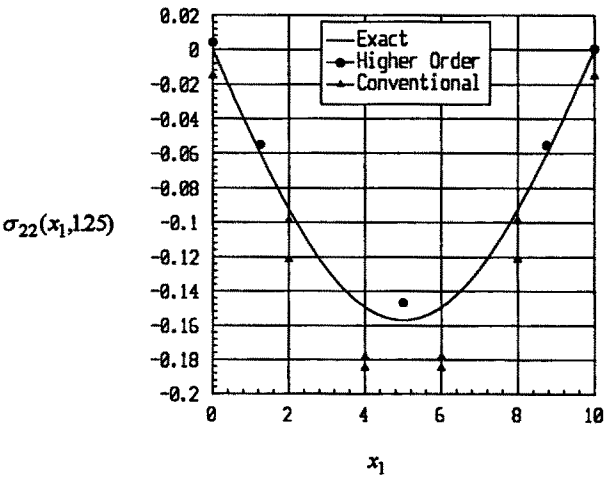

Fig. 8. Normal stress σ_{22} on the front face of the beam at $x_2 = 1.25$.

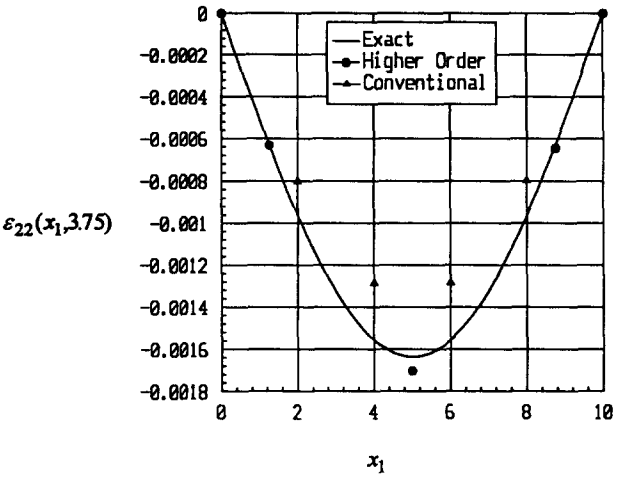

Fig. 9. Normal strain ε_{22} on the front face of the beam at $x_2 = 3.75$.

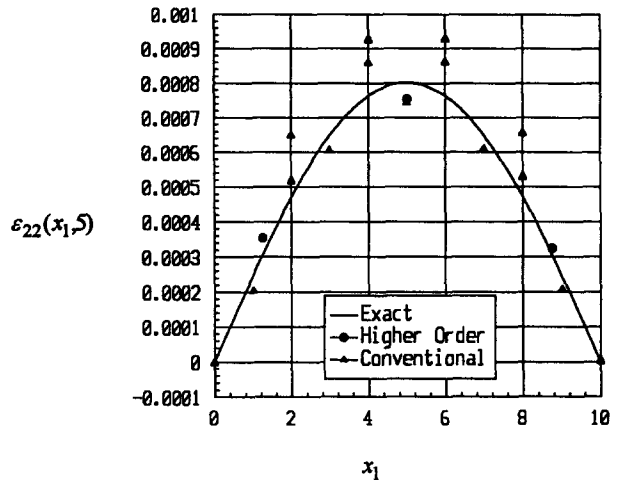

Fig. 10. Normal strain ε_{22} on the top face of the beam.

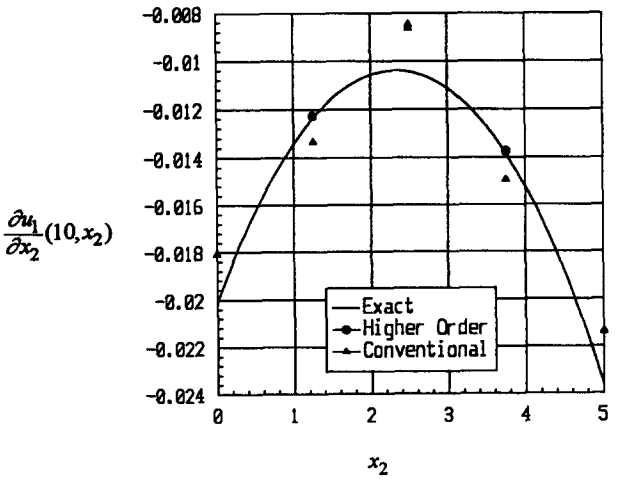

Fig. 11. Tangential displacement gradient on the right face of the beam.

analytical curve whereas the results for the conventional elements exhibit a considerable deviation.

It is important to mention that in the plots shown in Figs 7–11 all the data points correspond to values at the collocation points. For the higher order elements, these are the locations where they are expected to show its best performance since all the displacement gradients are obtained either directly from the solution to the integral equations or as parts of the boundary conditions. However, for the conventional elements, these are the places where they provide the worst values for the displacement gradients in the direction perpendicular to the element boundary.

DISCUSSION AND CONCLUSIONS

A general methodology to implement higher order elements for three-dimensional problems has been established. For elastostatic problems, the simultaneous collocation of the three displacement and the six tangent derivative boundary integral equations at the same boundary points proved to be computationally stable and allowed the use of the nodal values of the displacements, the tractions and their tangential derivatives as the degrees of freedom associated with the functional representation of the boundary variables. Since the tangential gradients of the displacements were incorporated in the formulation of the problem, their values at the functional nodes of the higher order elements were immediately retrieved from the boundary solution with an accuracy comparable to the primitive variables. Consequently, the tangential strains were directly obtained and all the stress components were easily computed using Hooke's law. In the case of the conventional elements, the tangent derivatives of the displacements (and consequently the tangential strain components) were established in a post-processing manner using the derivatives of the shape functions and the nodal values of the displacements and thus, less accurate values were found.

Although the number of degrees of freedom per node for the higher order elements is three times that for the conventional elements, the results obtained for a test problem show that this new type of elements is promising. For models with approximately the same number of boundary unknowns, the results provided by the higher order elements more closely matched the stresses, strains, and tangential displacement gradients predicted by the analytical solution. Of course, this fact is of practical importance since it reveals that a coarse mesh of higher order elements can be adequately used to model portions of the boundary where the field variables exhibit rapid changes. Also it should be pointed out that it is possible to use a combination of the conventional and the higher order elements for the discretization of the surface variables.

For the higher order elements in which some of the functional nodes are at the element edges, C^1 continuity of the displacements is only obtained at those particular points on the element interfaces. This situation, however, does not seem to pose difficulties to the evaluation of the regularized integrals associated with the derivative equations as long as the approximation of the boundary is sufficiently smooth at functional nodes that are shared by several elements. In fact, the conditions for the existence of the hypersingular integrals given by Günter (1967) show that the degree of continuity required from the density functions really depends on the smoothness of the surface at the source point.

REFERENCES

Aliabadi, M. H. and Rooke, D. P. (1991). *Numerical Fracture Mechanics*. Computational Mechanics Publications, Southampton.

Borisenko, A. I. and Tarapov, I. E. (1979). *Vector and Tensor Analysis with Applications*. Dover, New York.

Günter, N. M. (1967). *Potential Theory and its Applications to Basic Problems of Mathematical Physics*. Frederick Ungar, New York.

Hadamard, J. (1923). *Lectures on Cauchy's Problem in Linear Partial Differential Equations*. Yale University Press, New Haven.

Krishnasamy, G., Rizzo, F. J. and Rudolphi, T. J. (1992). Continuity requirements for density functions in the boundary integral equation method. *Computational Mech.* **9**, 267–284.

Krishnasamy, G., Rudolphi, T. J., Schmerr, L. W. and Rizzo, F. J. (1990). Hypersingular boundary integral equations: some applications in acoustics and elastic wave scattering. *ASME J. appl. Mech.* **57**, 404–414.
Little, R. Wm. (1973). *Elasticity*. Prentice-Hall, Englewood Cliffs, NJ.
Liu, Y. and Rizzo, F. J. (1991). Application of Overhauser C^1 continuous boundary elements to "hypersingular" BIE for 3-D acoustic wave problems. In *Boundary Elements XIII* (Edited by C. A. Brebbia and G. S. Gipson), pp. 957–966. Computational Mechanics Publications, Elsevier, Southampton.
Liu, Y. and Rudolphi, T. J. (1991) Some identities for fundamental solutions and their applications to non-singular boundary element formulations. *Engng Analysis Boundary Elements* **8**, 301–311.
Lutz, E., Gray, L. J. and Ingraffea, A. R. (1991) An overview of integration methods for hypersingular boundary integrals. In *Boundary Elements XIII* (Edited by C. A. Brebbia and G. S. Gipson), pp. 913–925. Computational Mechanics Publications, Elsevier, Southampton.
Muci-Küchler, K. H. and Rudolphi, T. J. (1993a). A weakly singular formulation of traction and tangent derivative boundary integral equations in three dimensional elasticity. *Engng Analysis Boundary Elements* **11**, 195–201.
Muci-Küchler, K. H. and Rudolphi, T. J. (1993b). Coincident collocation of displacement and tangent derivative boundary integral equations in elasticity. *Int. J. Numer. Meth. Engng* **36**, 2837–2849.
Rudolphi, T. J. (1989). Higher order elements and element enhancement by combined regular and hypersingular boundary integral equations. In *Int. Symp. on Boundary Element Methods* (Edited by B. S. Annigeri and K. Tseng), pp. 448–455. Springer, Berlin.
Rudolphi, T. J. (1991). The use of simple solutions in the regularization of hypersingular boundary integral equations. *Math. Comput. Modelling* **15**, 269–278.
Rudolphi, T. J. and Muci-Küchler, K. H. (1991). Consistent regularization of both kernels in hypersingular integral equations. In *Boundary Elements XIII* (Edited by C. A. Brebbia and G. S. Gipson), pp. 875–887. Computational Mechanics Publications, Elsevier, Southampton.
Sladek, V. and Sladek, J. (1986). Improved computation of stresses using the boundary element method. *Appl. Math. Modelling* **10**, 249–255.
Sladek, V., Sladek, J. and Tanaka, M. (1993). Regularization of hypersingular and nearly singular integrals in the potential theory and elasticity. *Int. J. Numer. Meth. Engng* **36**, 1609–1628.
Watson, J. O. (1986). Hermitian cubic and singular elements for plane strain. In *Developments in Boundary Element Methods* 4 (Edited by P. K. Banerjee and J. O. Watson), Chapter 1, pp. 1–28. Elsevier, London.

APPENDIX A: DETERMINATION OF THE SURFACE GRADIENTS

In the formulation of elements in three dimensions, it is customary to map the surface geometry into a local two-dimensional space characterized by two independent orthogonal coordinates, say η_1 and η_2. The surface gradients of a given function are readily determined through the use of tensor analysis, carrying out all required operations in the "global" (physical) space rather than in the local (mapped) one. For that purpose, as shown in Fig. A1, the global curvilinear coordinates (ρ^1, ρ^2, ρ^3) with basis vectors $(\mathbf{e}_1, \mathbf{e}_2, \mathbf{e}_3)$ and reciprocal basis vectors $(\mathbf{e}^1, \mathbf{e}^2, \mathbf{e}^3)$ are introduced such that the ρ^1 and ρ^2 coordinate curves in the global space correspond, respectively, to the η_1 and η_2 coordinate curves in the local space.

If $\mathbf{R}$ denotes the radius vector from the origin of the underlying rectangular coordinate system x_1, x_2, x_3 to a point on the element, the basis vectors $\mathbf{e}_1$ and $\mathbf{e}_2$ are

$$\mathbf{e}_\alpha = \frac{\partial \mathbf{R}}{\partial \rho^\alpha} \equiv \frac{\partial \mathbf{R}}{\partial \eta_\alpha} = \frac{\partial x_k}{\partial \eta_\alpha} \mathbf{i}_k. \tag{A1}$$

The directional derivative of a scalar field φ in the direction of a unit vector $\mathbf{p}$ is given by [see, for example, Borisenko and Tarapov (1979)]

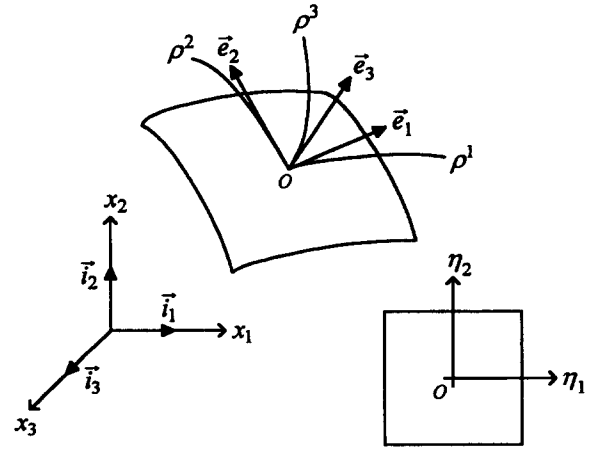

Fig. A1. Coordinate systems associated with a surface boundary element.

$$\frac{d\varphi}{dp} = \mathbf{p}\cdot\nabla\varphi = \mathbf{p}\cdot\left[\mathbf{e}^1\frac{\partial\varphi}{\partial\rho^1} + \mathbf{e}^2\frac{\partial\varphi}{\partial\rho^2} + \mathbf{e}^3\frac{\partial\varphi}{\partial\rho^3}\right], \tag{A2}$$

where $\partial\varphi/\partial\rho^i$ are the covariant components of the gradient vector $\nabla\varphi$. However, if one chooses a unit vector $\mathbf{p}$ tangent to the surface, then the above expression becomes

$$\frac{d\varphi}{dp} = (\mathbf{p}\cdot\mathbf{e}^1)\frac{\partial\varphi}{\partial\rho^1} + (\mathbf{p}\cdot\mathbf{e}^2)\frac{\partial\varphi}{\partial\rho^2}. \tag{A3}$$

If the covariant components of the metric tensor are denoted by $g_{ij} = \mathbf{e}_i\cdot\mathbf{e}_j$, it can be shown that

$$\begin{Bmatrix}\mathbf{p}\cdot\mathbf{e}^1\\ \mathbf{p}\cdot\mathbf{e}^2\end{Bmatrix} = \begin{bmatrix}g_{11} & g_{12}\\ g_{21} & g_{22}\end{bmatrix}^{-1}\begin{Bmatrix}\mathbf{p}\cdot\mathbf{e}_1\\ \mathbf{p}\cdot\mathbf{e}_2\end{Bmatrix}, \tag{A4}$$

where

$$g_{\alpha\beta} = \frac{\partial x_k}{\partial\eta_\alpha}\frac{\partial x_k}{\partial\eta_\beta}. \tag{A5}$$

Using eqn (A4) and recalling that $\rho^1 \equiv \eta_1$ and $\rho^2 \equiv \eta_2$, eqn (A3) can be written as

$$\frac{d\varphi}{dp} = \frac{1}{G}\left[(g_{22}\mathbf{e}_1 - g_{12}\mathbf{e}_2)\frac{\partial\varphi}{\partial\eta_1} + (g_{11}\mathbf{e}_2 - g_{21}\mathbf{e}_1)\frac{\partial\varphi}{\partial\eta_2}\right]\cdot\mathbf{p}, \tag{A6}$$

where $G = \det(g_{\alpha\beta})$.

If one identifies u_i with φ and if $\mathbf{s}_1$ and $\mathbf{s}_2$ are orthogonal unit tangent vectors such that $\mathbf{s}_1\times\mathbf{s}_2 = \mathbf{n}$, then eqn (A6) establishes the surface gradients of the rectangular components of the displacement vector $\mathbf{u}$ as

$$\frac{\partial u_i}{\partial s_\alpha} = \frac{1}{G}\left[(g_{22}\mathbf{e}_1 - g_{12}\mathbf{e}_2)\frac{\partial u_i}{\partial\eta_1} + (g_{11}\mathbf{e}_2 - g_{21}\mathbf{e}_1)\frac{\partial u_i}{\partial\eta_2}\right]\cdot\mathbf{s}_\alpha. \tag{A7}$$

From eqns (A1), (A5), and (A7) it is evident that to compute the values of $\partial u_i/\partial s_\alpha$ the quantities $\partial x_i/\partial\eta_\alpha$ and $\partial u_i/\partial\eta_\alpha$ need to be determined.

In general, the element surface is approximated by

$$x_i = \sum_{J=1}^{n} N_J(\eta_1,\eta_2)[x_i]^J, \quad i = 1,2,3, \tag{A8}$$

where n is the number of geometric nodes, $N_J(\eta_1,\eta_2)$ are the geometric shape functions and $[x_i]^J$ denotes the ith coordinate of the Jth geometric node. Consequently

$$\frac{\partial x_i}{\partial\eta_\alpha} = \sum_{J=1}^{n}\frac{\partial N_J}{\partial\eta_\alpha}(\eta_1,\eta_2)[x_i]^J, \quad i = 1,2,3. \tag{A9}$$

Similarly, the approximation for the displacement components u_i in a conventional element with m functional nodes would be

$$u_i = \sum_{J=1}^{m} M_J(\eta_1,\eta_2)[u_i]^J, \quad i = 1,2,3, \tag{A10}$$

where $M_J(\eta_1,\eta_2)$ are the shape functions associated with the field variables and the notation $[\cdot]^J$ is used to specify quantities evaluated at the Jth functional node. Thus

$$\frac{\partial u_i}{\partial\eta_\alpha} = \sum_{J=1}^{m}\frac{\partial M_J}{\partial\eta_\alpha}(\eta_1,\eta_2)[u_i]^J, \quad i = 1,2,3. \tag{A11}$$

APPENDIX B: SHAPE FUNCTIONS FOR THE HIGHER ORDER ELEMENTS

The procedure used to determine the "geometry independent" shape functions $\hat{H}_0^J$, $\hat{H}_1^J$, and $\hat{H}_2^J$ ($J = 1,2,\ldots,m$) is similar to that of the finite element method in the derivation of C^1 continuous two-dimensional elements. Once the geometry of an element has been defined in the local space characterized by the parametric coordinates η_1 and η_2, the first step is to specify the total number of functional nodes associated with the element and the specific coordinates for each node. Next, the type of function to be used for the approximation of the field variables is selected and then conditions (21)–(23) are applied to find the particular set of interpolation functions. In what follows several sets of polynomial shape functions for quadrilateral elements with sides at $\eta_1 = \pm 1$ and $\eta_2 = \pm 1$ are presented.

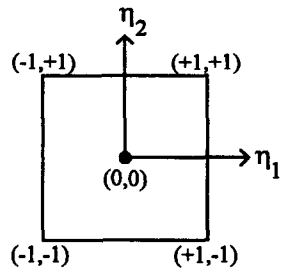

Fig. B1. Discontinuous linear element.

Discontinuous linear element

The simplest higher order element is the one shown in Fig. B1. There is only one interior functional node located at $(\eta_1, \eta_2) = (0, 0)$ and three shape functions to approximate the field variables: $\hat{H}^1_0(\eta_1, \eta_2) = 1$, $\hat{H}^1_1(\eta_1, \eta_2) = \eta_1$ and $\hat{H}^1_2(\eta_1, \eta_2) = \eta_2$. This element can be viewed as the counterpart of the constant element used in the conventional boundary element method. Although it provides a linear variation for the displacement and traction components, the surface gradients of these quantities will be represented as constant values.

Incomplete quartic elements

A family of four node, continuous, partially continuous and discontinuous elements is shown in Fig. B2. The six elements shown have several common characteristics. All elements have four functional nodes and the 12 shape functions can be constructed using an incomplete quartic polynomial in which the terms η_1^4, $\eta_1^2\eta_2^2$, and η_2^4 have been excluded. The shape functions corresponding to each element are as follows.

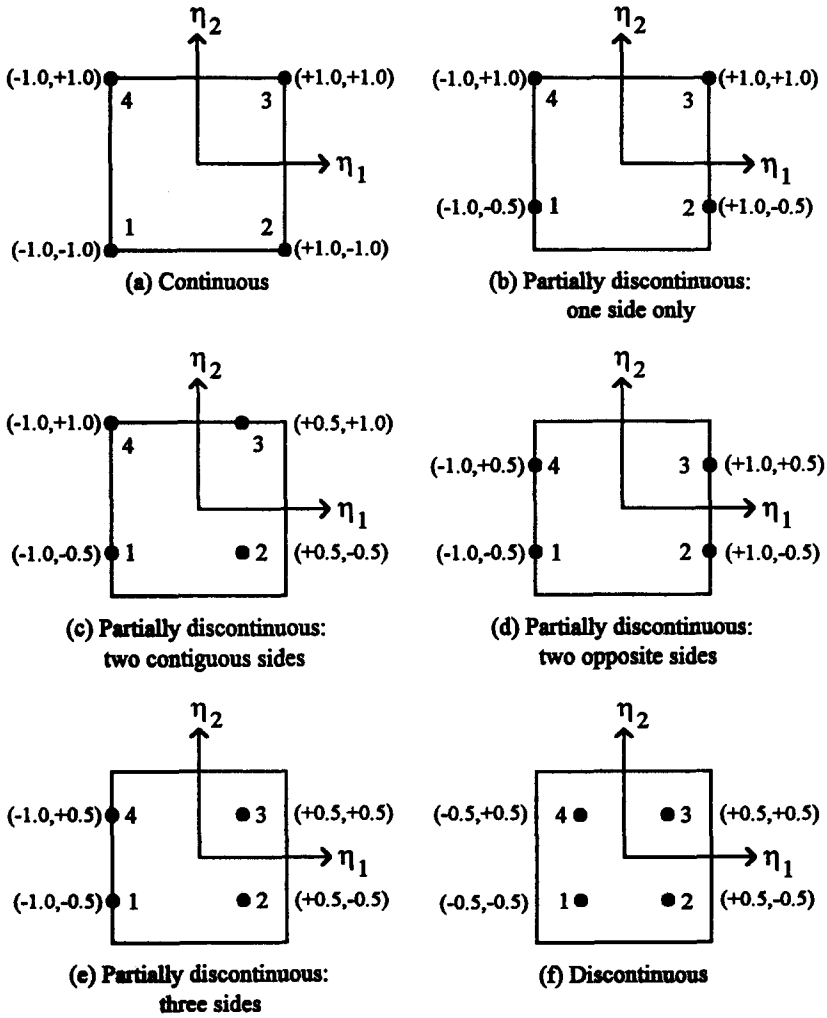

Fig. B2. Incomplete quartic elements.

(*a*) *Continuous incomplete quartic element.*

$$\hat{H}^1_0(\eta_1,\eta_2) = -\tfrac{1}{8}(\eta_1-1)(\eta_2-1)[\eta_1(\eta_1+1)+\eta_2(\eta_2+1)-2]$$
$$\hat{H}^1_1(\eta_1,\eta_2) = -\tfrac{1}{8}(\eta_1+1)(\eta_2-1)(\eta_1-1)^2$$
$$\hat{H}^1_2(\eta_1,\eta_2) = -\tfrac{1}{8}(\eta_1-1)(\eta_2+1)(\eta_2-1)^2$$
$$\hat{H}^2_0(\eta_1,\eta_2) = \tfrac{1}{8}(\eta_1+1)(\eta_2-1)[\eta_1(\eta_1-1)+\eta_2(\eta_2+1)-2]$$
$$\hat{H}^2_1(\eta_1,\eta_2) = -\tfrac{1}{8}(\eta_1-1)(\eta_2-1)(\eta_1+1)^2$$
$$\hat{H}^2_2(\eta_1,\eta_2) = \tfrac{1}{8}(\eta_1+1)(\eta_2+1)(\eta_2-1)^2$$
$$\hat{H}^3_0(\eta_1,\eta_2) = -\tfrac{1}{8}(\eta_1+1)(\eta_2+1)[\eta_1(\eta_1-1)+\eta_2(\eta_2-1)-2]$$
$$\hat{H}^3_1(\eta_1,\eta_2) = \tfrac{1}{8}(\eta_1-1)(\eta_2+1)(\eta_1+1)^2$$
$$\hat{H}^3_2(\eta_1,\eta_2) = \tfrac{1}{8}(\eta_1+1)(\eta_2-1)(\eta_2+1)^2$$
$$\hat{H}^4_0(\eta_1,\eta_2) = \tfrac{1}{8}(\eta_1-1)(\eta_2+1)[\eta_1(\eta_1+1)+\eta_2(\eta_2-1)-2]$$
$$\hat{H}^4_1(\eta_1,\eta_2) = \tfrac{1}{8}(\eta_1+1)(\eta_2+1)(\eta_1-1)^2$$
$$\hat{H}^4_2(\eta_1,\eta_2) = -\tfrac{1}{8}(\eta_1-1)(\eta_2-1)(\eta_2+1)^2.$$

(*b*) *Incomplete quartic element discontinuous on one side.*

$$\hat{H}^1_0(\eta_1,\eta_2) = -\tfrac{1}{54}(\eta_1-1)(\eta_2-1)[9\eta_1(\eta_1+1)+4\eta_2(4\eta_2+1)-20]$$
$$\hat{H}^1_1(\eta_1,\eta_2) = -\tfrac{1}{6}(\eta_1+1)(\eta_2-1)(\eta_1-1)^2$$
$$\hat{H}^1_2(\eta_1,\eta_2) = -\tfrac{1}{9}(\eta_1-1)(2\eta_2+1)(\eta_2-1)^2$$
$$\hat{H}^2_0(\eta_1,\eta_2) = \tfrac{1}{54}(\eta_1+1)(\eta_2-1)[9\eta_1(\eta_1-1)+4\eta_2(4\eta_2+1)-20]$$
$$\hat{H}^2_1(\eta_1,\eta_2) = -\tfrac{1}{6}(\eta_1-1)(\eta_2-1)(\eta_1+1)^2$$
$$\hat{H}^2_2(\eta_1,\eta_2) = \tfrac{1}{9}(\eta_1+1)(2\eta_2+1)(\eta_2-1)^2$$
$$\hat{H}^3_0(\eta_1,\eta_2) = -\tfrac{1}{108}(\eta_1+1)(2\eta_2+1)[9\eta_1(\eta_1-1)+4\eta_2(4\eta_2-5)-14]$$
$$\hat{H}^3_1(\eta_1,\eta_2) = \tfrac{1}{12}(\eta_1-1)(2\eta_2+1)(\eta_1+1)^2$$
$$\hat{H}^3_2(\eta_1,\eta_2) = \tfrac{1}{18}(\eta_1+1)(\eta_2-1)(2\eta_2+1)^2$$
$$\hat{H}^4_0(\eta_1,\eta_2) = \tfrac{1}{108}(\eta_1-1)(2\eta_2+1)[9\eta_1(\eta_1+1)+4\eta_2(4\eta_2-5)-14]$$
$$\hat{H}^4_1(\eta_1,\eta_2) = \tfrac{1}{12}(\eta_1+1)(2\eta_2+1)(\eta_1-1)^2$$
$$\hat{H}^4_2(\eta_1,\eta_2) = -\tfrac{1}{18}(\eta_1-1)(\eta_2-1)(2\eta_2+1)^2.$$

(*c*) *Incomplete quartic element discontinuous on two contiguous sides.*

$$\hat{H}^1_0(\eta_1,\eta_2) = -\tfrac{4}{81}(2\eta_1-1)(\eta_2-1)[\eta_1(4\eta_1+5)+\eta_2(4\eta_2+1)-4]$$
$$\hat{H}^1_1(\eta_1,\eta_2) = -\tfrac{2}{27}(\eta_1+1)(\eta_2-1)(2\eta_1-1)^2$$
$$\hat{H}^1_2(\eta_1,\eta_2) = -\tfrac{2}{27}(2\eta_1-1)(2\eta_2+1)(\eta_2-1)^2$$
$$\hat{H}^2_0(\eta_1,\eta_2) = \tfrac{4}{81}(\eta_1+1)(\eta_2-1)[2\eta_1(4\eta_1-1)+2\eta_2(4\eta_2+1)-11]$$
$$\hat{H}^2_1(\eta_1,\eta_2) = -\tfrac{4}{27}(2\eta_1-1)(\eta_2-1)(\eta_1+1)^2$$
$$\hat{H}^2_2(\eta_1,\eta_2) = \tfrac{4}{27}(\eta_1+1)(2\eta_2+1)(\eta_2-1)^2$$
$$\hat{H}^3_0(\eta_1,\eta_2) = -\tfrac{4}{81}(\eta_1+1)(2\eta_2+1)[\eta_1(4\eta_1-1)+\eta_2(4\eta_2-5)-4]$$
$$\hat{H}^3_1(\eta_1,\eta_2) = \tfrac{2}{27}(2\eta_1-1)(2\eta_2+1)(\eta_1+1)^2$$
$$\hat{H}^3_2(\eta_1,\eta_2) = \tfrac{2}{27}(\eta_1+1)(\eta_2-1)(2\eta_2+1)^2$$
$$\hat{H}^4_0(\eta_1,\eta_2) = \tfrac{1}{81}(2\eta_1-1)(2\eta_2+1)[2\eta_1(4\eta_1+5)+2\eta_2(4\eta_2-5)-5]$$
$$\hat{H}^4_1(\eta_1,\eta_2) = \tfrac{1}{27}(\eta_1+1)(2\eta_2+1)(2\eta_1-1)^2$$
$$\hat{H}^4_2(\eta_1,\eta_2) = -\tfrac{1}{27}(2\eta_1-1)(\eta_2-1)(2\eta_2+1)^2.$$

(*d*) *Incomplete quartic element discontinuous on two opposite sides.*

$$\hat{H}^1_0(\eta_1,\eta_2) = -\tfrac{1}{8}(\eta_1-1)(2\eta_2-1)[\eta_1(\eta_1+1)+2\eta_2(2\eta_2+1)-2]$$
$$\hat{H}^1_1(\eta_1,\eta_2) = -\tfrac{1}{8}(\eta_1+1)(2\eta_2-1)(\eta_1-1)^2$$

$$\hat{H}^1_2(\eta_1,\eta_2) = -\tfrac{1}{16}(\eta_1-1)(2\eta_2+1)(2\eta_2-1)^2$$
$$\hat{H}^2_0(\eta_1,\eta_2) = \tfrac{1}{8}(\eta_1+1)(2\eta_2-1)[\eta_1(\eta_1-1)+2\eta_2(2\eta_2+1)-2]$$
$$\hat{H}^2_1(\eta_1,\eta_2) = -\tfrac{1}{8}(\eta_1-1)(2\eta_2-1)(\eta_1+1)^2$$
$$\hat{H}^2_2(\eta_1,\eta_2) = \tfrac{1}{16}(\eta_1+1)(2\eta_2+1)(2\eta_2-1)^2$$
$$\hat{H}^3_0(\eta_1,\eta_2) = -\tfrac{1}{8}(\eta_1+1)(2\eta_2+1)[\eta_1(\eta_1-1)+2\eta_2(2\eta_2-1)-2]$$
$$\hat{H}^3_1(\eta_1,\eta_2) = \tfrac{1}{8}(\eta_1-1)(2\eta_2+1)(\eta_1+1)^2$$
$$\hat{H}^3_2(\eta_1,\eta_2) = \tfrac{1}{16}(\eta_1+1)(2\eta_2-1)(2\eta_2+1)^2$$
$$\hat{H}^4_0(\eta_1,\eta_2) = \tfrac{1}{8}(\eta_1-1)(2\eta_2+1)[\eta_1(\eta_1+1)+2\eta_2(2\eta_2-1)-2]$$
$$\hat{H}^4_1(\eta_1,\eta_2) = \tfrac{1}{8}(\eta_1+1)(2\eta_2+1)(\eta_1-1)^2$$
$$\hat{H}^4_2(\eta_1,\eta_2) = -\tfrac{1}{16}(\eta_1-1)(2\eta_2-1)(2\eta_2+1)^2.$$

(e) Incomplete quartic element discontinuous on three sides.

$$\hat{H}^1_0(\eta_1,\eta_2) = -\tfrac{1}{54}(2\eta_1-1)(2\eta_2-1)[2\eta_1(4\eta_1+5)+9\eta_2(2\eta_2+1)-7]$$
$$\hat{H}^1_1(\eta_1,\eta_2) = -\tfrac{1}{18}(\eta_1+1)(2\eta_2-1)(2\eta_1-1)^2$$
$$\hat{H}^1_2(\eta_1,\eta_2) = -\tfrac{1}{24}(2\eta_1-1)(2\eta_2+1)(2\eta_2-1)^2$$
$$\hat{H}^2_0(\eta_1,\eta_2) = \tfrac{1}{27}(\eta_1+1)(2\eta_2-1)[2\eta_1(4\eta_1-1)+9\eta_2(2\eta_2+1)-10]$$
$$\hat{H}^2_1(\eta_1,\eta_2) = -\tfrac{1}{9}(2\eta_1-1)(2\eta_2-1)(\eta_1+1)^2$$
$$\hat{H}^2_2(\eta_1,\eta_2) = \tfrac{1}{12}(\eta_1+1)(2\eta_2+1)(2\eta_2-1)^2$$
$$\hat{H}^3_0(\eta_1,\eta_2) = -\tfrac{1}{27}(\eta_1+1)(2\eta_2+1)[2\eta_1(4\eta_1-1)+9\eta_2(2\eta_2-1)-10]$$
$$\hat{H}^3_1(\eta_1,\eta_2) = \tfrac{1}{9}(2\eta_1-1)(2\eta_2+1)(\eta_1+1)^2$$
$$\hat{H}^3_2(\eta_1,\eta_2) = \tfrac{1}{12}(\eta_1+1)(2\eta_2-1)(2\eta_2+1)^2$$
$$\hat{H}^4_0(\eta_1,\eta_2) = \tfrac{1}{54}(2\eta_1-1)(2\eta_2+1)[2\eta_1(4\eta_1+5)+9\eta_2(2\eta_2-1)-7]$$
$$\hat{H}^4_1(\eta_1,\eta_2) = \tfrac{1}{18}(\eta_1+1)(2\eta_2+1)(2\eta_1-1)^2$$
$$\hat{H}^4_2(\eta_1,\eta_2) = -\tfrac{1}{24}(2\eta_1-1)(2\eta_2-1)(2\eta_2+1)^2.$$

(f) Discontinuous incomplete quartic element.

$$\hat{H}^1_0(\eta_1,\eta_2) = -\tfrac{1}{4}(2\eta_1-1)(2\eta_2-1)[\eta_1(2\eta_1+1)+\eta_2(2\eta_2+1)-1]$$
$$\hat{H}^1_1(\eta_1,\eta_2) = -\tfrac{1}{16}(2\eta_1+1)(2\eta_2-1)(2\eta_1-1)^2$$
$$\hat{H}^1_2(\eta_1,\eta_2) = -\tfrac{1}{16}(2\eta_1-1)(2\eta_2+1)(2\eta_2-1)^2$$
$$\hat{H}^2_0(\eta_1,\eta_2) = \tfrac{1}{4}(2\eta_1+1)(2\eta_2-1)[\eta_1(2\eta_1-1)+\eta_2(2\eta_2+1)-1]$$
$$\hat{H}^2_1(\eta_1,\eta_2) = -\tfrac{1}{16}(2\eta_1-1)(2\eta_2-1)(2\eta_1+1)^2$$
$$\hat{H}^2_2(\eta_1,\eta_2) = \tfrac{1}{16}(2\eta_1+1)(2\eta_2+1)(2\eta_2-1)^2$$
$$\hat{H}^3_0(\eta_1,\eta_2) = -\tfrac{1}{4}(2\eta_1+1)(2\eta_2+1)[\eta_1(2\eta_1-1)+\eta_2(2\eta_2-1)-1]$$
$$\hat{H}^3_1(\eta_1,\eta_2) = \tfrac{1}{16}(2\eta_1-1)(2\eta_2+1)(2\eta_1+1)^2$$
$$\hat{H}^3_2(\eta_1,\eta_2) = \tfrac{1}{16}(2\eta_1+1)(2\eta_2-1)(2\eta_2+1)^2$$
$$\hat{H}^4_0(\eta_1,\eta_2) = \tfrac{1}{4}(2\eta_1-1)(2\eta_2+1)[\eta_1(2\eta_1+1)+\eta_2(2\eta_2-1)-1]$$
$$\hat{H}^4_1(\eta_1,\eta_2) = \tfrac{1}{16}(2\eta_1+1)(2\eta_2+1)(2\eta_1-1)^2$$
$$\hat{H}^4_2(\eta_1,\eta_2) = -\tfrac{1}{16}(2\eta_1-1)(2\eta_2-1)(2\eta_2+1)^2.$$